ACCSCIENCE PUBLISHING

Journal of Seismic Exploration

ARTICLE

Unscaled generalized S-transform and its applications on seismic attenuation delineation: A case study in the Ordos Basin, Northwest China

Wenlong Jiao[1], Naihao Liu[2]*, Yongxiang Jiang[1], Jun Yang[3], and Wei Zhao[3]

[1]Department of Geophysics, PetroChina Yumen Oilfield Company, Jiuquan, Gansu, China

[2]School of Information and Communications Engineering, Xi'an Jiaotong University, Xi'an, Shaanxi, China

[3]Exploration and Development Research Institute, PetroChina Yumen Oilfield Company, Jiuquan, Gansu, China

(This article belongs to the *Special Issue: Advanced Artificial Intelligence Theories and Methods for Seismic Exploration*)

Abstract

Seismic attenuation estimation is an important tool for hydrocarbon identification and reservoir characterization. Conventional time–frequency (TF) methods, particularly the S-transform (ST), are widely applied but suffer from a systematic dominant-frequency shift and fixed TF resolution, which may reduce the accuracy of attenuation analysis. To address these limitations, we introduce the unscaled generalized ST (UGST) and apply it to field seismic data from the Ordos Basin in Northwest China to qualitatively estimate attenuation. The UGST corrects the frequency shift inherent in the standard ST and introduces two tunable parameters that enable flexible adjustment of TF resolution to better match local seismic responses. Application to a three-dimensional seismic dataset demonstrates that the UGST produces TF spectra with improved readability and accurate frequency localization, resulting in a reduction of approximately 10 Hz in dominant frequency error compared to ST. The attenuation attributes derived from UGST show strong correspondence with known gas-bearing intervals, as verified by well-log data. The derived attenuation attributes show strong correspondence with gas-bearing intervals, with anomaly overlap rates exceeding 85% relative to well-log fluid indicators. These results indicate that the UGST provides a robust and effective approach for delineating seismic attenuation, offering practical value for reservoir characterization in exploration geophysics.

Keywords: Seismic attenuation estimation; Time–frequency analysis; Unscaled generalized S-transform; Reservoir characterization

***Corresponding author:**
Naihao Liu
(naihao_liu@mail.xjtu.edu.cn)

Citation: Jiao W, Liu N, Jiang Y, Yang J, Zhao W. Unscaled generalized S-transform and its applications on seismic attenuation delineation: A case study in the Ordos Basin, Northwest China. *J Seismic Explor*. doi: 10.36922/JSE025450106

Received: November 7, 2025

Revised: January 7, 2026

Accepted: January 12, 2026

Published online: February 10, 2026

1. Introduction

In hydrocarbon exploration, seismic attenuation analysis is an essential technique for fluid identification and reservoir characterization.[1-3] The physical basis of this approach

lies in the observation that when seismic waves propagate through hydrocarbon-bearing formations, high-frequency components generally undergo greater energy attenuation than low-frequency ones.[4,5] This frequency-dependent amplitude loss provides a useful indicator for direct hydrocarbon detection, particularly in gas-saturated porous media.[6-8] Conventional qualitative attenuation analysis methods typically employ time–frequency (TF) analysis techniques, in which attenuation anomalies are identified by comparing energy variations across different frequency components.[9,10]

The development of qualitative attenuation estimation has advanced in parallel with improvements in TF analysis.[11,12] Early studies used basic spectral decomposition methods, comparing amplitude spectra within selected time windows to detect frequency anomalies. Although conceptually simple, these approaches suffered from limited resolution and an inability to effectively track temporal changes in spectral content. Advances in TF analysis led to sophisticated techniques, including the continuous wavelet transform and various adaptive TF representations. These methods offer improved capabilities for visualizing and quantifying frequency-dependent amplitude variations.[13-15] Moreover, excellent TF analysis tools have been proposed in recent years to address various practical issues, such as the synchrosqueezing transform[16] and sparse transform.[17,18] Although they can improve the TF resolution, these methods have various limitations in real applications, such as the difficult parameter selection, the high computational cost, and the high requirements for actual data.[18,19] Similar challenges are encountered in other signal processing domains, where advanced techniques are developed for weak-signal enhancement[20] and adaptive noise suppression.[21] These approaches, while promising, often involve complex parameterization that may limit their direct applicability to large-scale seismic datasets.

Among various TF analysis methods, the S-transform (ST) has attracted considerable attention for its distinctive TF resolution characteristics.[22,23] Unlike the fixed window length in the short-time fourier transform, the ST employs a frequency-adaptive Gaussian window, providing higher frequency resolution at low frequencies and better time resolution at high frequencies. This property of progressive resolution has led to its wide application in seismic signal analysis, especially for detecting thin beds and characterizing complex stratigraphic features.[9,24] Its ability to provide frequency-dependent resolution makes it particularly suitable for seismic attenuation analysis, where both temporal precision and frequency discrimination are essential.[23,25] Furthermore, it can benefit from several fast algorithms, significantly promoting its practical applications.[26-29]

However, the conventional ST exhibits a dominant frequency shift, in which the peak frequency in the computed spectrum deviates from the true frequency. This shift, caused by the frequency scaling of the Gaussian window, can affect the accuracy of attenuation estimation.[30] When comparing high- and low-frequency components for attenuation analysis, such frequency shifts may introduce systematic errors, leading to misinterpretation of attenuation anomalies or failure to detect subtle hydrocarbon indicators.[19,31] To mitigate this problem, researchers proposed the unscaled ST (UST). The UST modifies the Gaussian window function to correct the dominant frequency shift while preserving the adaptive nature of the original ST.[30] This adjustment ensures that the estimated frequencies more accurately represent the true spectral content of the signal. Nevertheless, the UST retains the same resolution characteristics as the conventional ST, which cannot be flexibly tuned for different geological targets or data types. This limitation becomes critical in complex reservoir characterization, where geological targets often demand varying TF resolutions for optimal interpretation. For example, detecting thin layers may require higher temporal resolution, whereas distinguishing subtle stratigraphic features benefits from improved frequency resolution.[32,33] The inability to adapt transform parameters to specific geological contexts constrains practical applications, particularly in heterogeneous reservoirs where attenuation behavior can vary significantly.[34,35]

The study area, located at the Ordos Basin, Northwest China, presents a compelling case for testing advanced attenuation estimation methods. This region contains complex fluvial-deltaic systems characterized by thin interbedded sandstones and shales, with reservoir thickness often below the tuning thickness. Extensive faulting complicates the structural setting, creating compartmentalized reservoirs with varying fluid contacts. Although previous exploration has confirmed the commercial hydrocarbon accumulations, reservoir delineation remains challenging. This is primarily due to complex pore-fluid distributions and subtle seismic responses, which necessitate advanced analytical techniques. These geological complexities necessitate advanced analytical techniques capable of resolving subtle attenuation anomalies associated with hydrocarbon presence.

In this context, we propose applying the unscaled generalized ST (UGST) to estimate attenuation qualitatively in these challenging seismic data. The UGST maintains frequency accuracy while enabling flexible control of TF resolution through adjustable parameters. This enhanced flexibility allows for optimization of the TF representation

according to specific geological objectives and data characteristics. We established a comprehensive workflow for qualitative attenuation analysis using the UGST, incorporating optimized parameter selection, frequency-component extraction, and attenuation calculation. The workflow is validated using comprehensive three-dimensional (3D) seismic data from the Ordos Basin, Northwest China, supported by well log information and production data for verification. Practical applications demonstrate that, compared to conventional methods, UGST yields more interpretable TF spectra and more reliable attenuation estimations. The method identifies attenuation anomalies in known hydrocarbon-bearing zones and provides improved resolution of thin reservoir units. This approach offers an effective technical solution for reservoir characterization under complex geological conditions, particularly in challenging exploration settings where conventional attributes provide ambiguous results. The successful application of UGST-based attenuation analysis in this study highlights its potential as a robust tool for reservoir characterization and reduction of exploration risk in geologically complex areas.

2. Methodology

2.1. Theoretical foundation of UGST

The UGST represents a significant advancement in TF analysis, specifically designed to overcome the limitations of conventional methods while preserving accurate frequency representation. The development of UGST builds upon the foundation of the standard ST, which itself marked an important evolution in TF analysis methodology.

The conventional ST of a seismic signal $x(t)$ is defined as **Equation (1)**:

$$ST(\tau,f)=\int_{-\infty}^{+\infty}x(t)\frac{|f|}{\sqrt{2\pi}}e^{-\frac{(t-\tau)^2f^2}{2}}e^{-i2\pi ft}dt \tag{1}$$

Where f and t represent frequency and time variables, and τ denotes the time shifting variable. While ST provides a frequency-adaptive analysis window, it suffers from a systematic dominant frequency shift due to the scaling factor $|f|$ in the Gaussian window.

To address this frequency shift issue, the UST is introduced with the modified formulation,[30] written as **Equation (2)**:

$$UST(\tau,f)=\int_{-\infty}^{+\infty}x(t)\frac{1}{\sqrt{2\pi}}e^{-\frac{(t-\tau)^2f^2}{2}}e^{-i2\pi ft}dt \tag{2}$$

The UST removes the frequency scaling factor from the normalization term $|f|/\sqrt{2\pi}$ of the window function based on the conventional ST. This modification prevents a shift in the dominant frequency toward higher frequencies. Meanwhile, the UST retains the frequency scaling in the exponential term, preserving its ability to adaptively adjust TF localization characteristics. The removal of the scaling factor $|f|$ in UST's normalization term addresses a fundamental limitation of standard ST. In conventional ST, this frequency-dependent scaling introduces a systematic bias in spectral localization, shifting estimated frequencies upward. UST eliminates this bias by decoupling the normalization from frequency scaling, thereby providing accurate frequency representation while preserving the adaptive window mechanism.

Building on UST, we propose the UGST, which incorporates additional parameters to enable flexible adjustment of TF resolution while maintaining frequency accuracy. The UGST is defined as **Equation (3)**:

$$UGST(\tau,f)=\int_{-\infty}^{+\infty}x(t)\frac{1}{\sqrt{2\pi}}e^{-\frac{(t-\tau)^2(kf^p)^2}{2}}e^{-i2\pi ft}dt \tag{3}$$

Where k and p are two tunable parameters to control the window of our transform. Next, we also have the UGST in the frequency domain, denoted as **Equation (4)**:

$$\begin{aligned}UGST(\tau,f)&=\int_{-\infty}^{+\infty}x(t)\frac{1}{\sqrt{2\pi}}e^{-\frac{(t-\tau)^2(kf^p)^2}{2}}e^{-i2\pi ft}dt\\&=x(\tau)e^{-i2\pi f\tau}\circledast g(\tau)\\&=IFT\left\{\hat{x}(\xi+f)\hat{g}(\xi)\right\}\\&=\int_{-\infty}^{+\infty}\hat{x}(\xi+f)\frac{1}{k|f|^p}e^{-\frac{2\pi^2\xi^2}{(kf^p)^2}}e^{i2\pi\xi\tau}d\xi\end{aligned} \tag{4}$$

Through this systematic approach, UGST leverages both accurate frequency localization and flexible resolution control to generate reliable attenuation estimates. By integrating geological constraints through reference-layer normalization, the method effectively distinguishes fluid-related attenuation from lithological effects, providing a robust tool for reservoir characterization.

2.2. Qualitative attenuation estimation workflow

We developed a workflow for qualitative attenuation characterization based on the proposed UGST, as shown in Figure 1. The workflow leverages the stronger attenuation of the high-frequency component relative to the low-frequency component and compares the difference between the two components to directly indicate the region of strong attenuation.[36,37]

We first denoted the two-dimensional seismic data with $d(x,t)$, where x and t represent the CDP number and

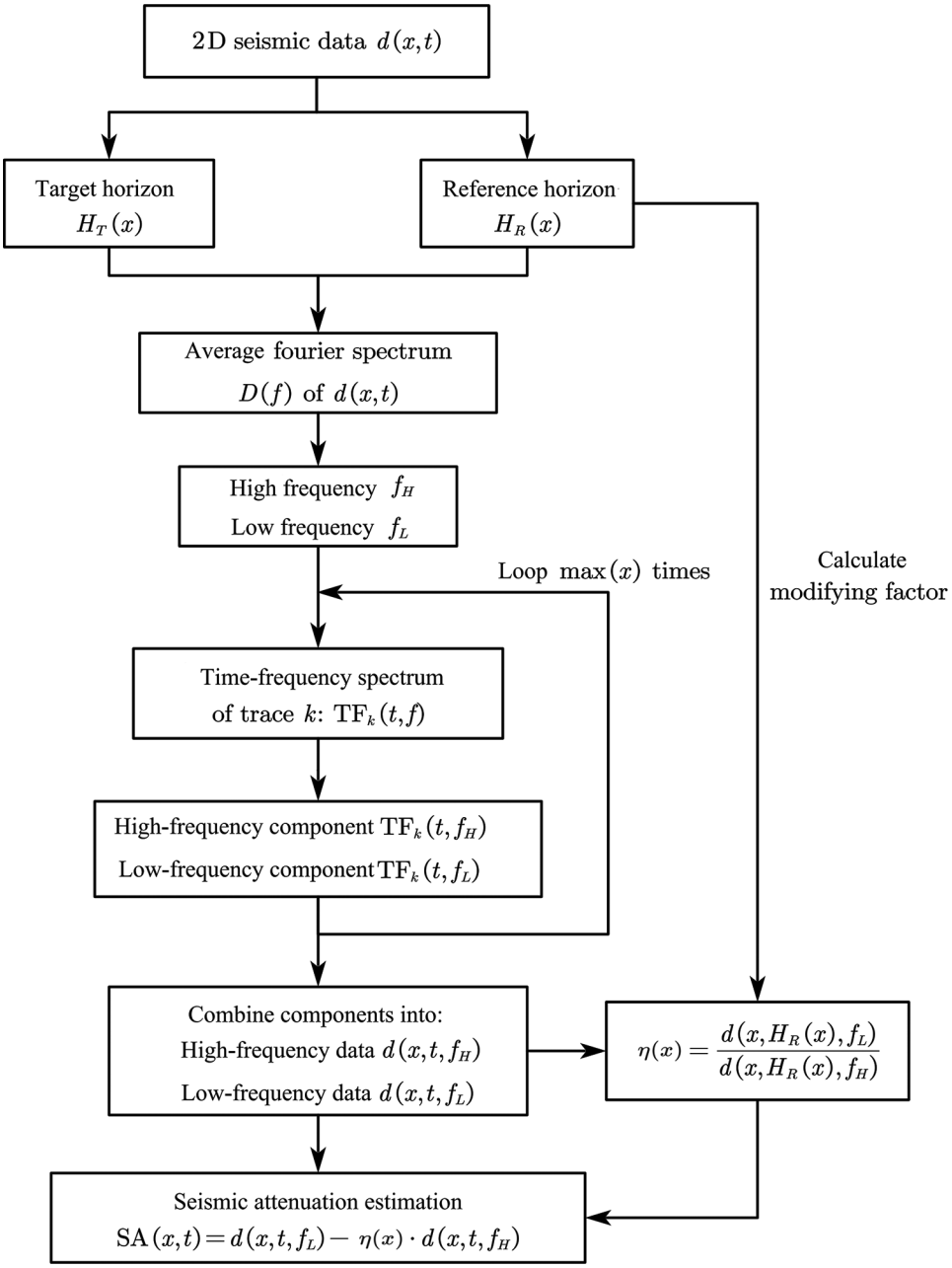

Figure 1. The proposed workflow of seismic attenuation characterization based on the proposed unscaled generalized S-transform
Abbreviations: 2D: Two-dimensional; SA: Seismic attenuation.

the time index. $H_T(x)$ is the target layer and $H_R(x)$ is the reference layer. Next, we selected the high frequency and the low frequency based on the average Fourier spectrum $D(f)$ of $d(x,t)$. Notably, f should be included in the effective frequency band. Then, we adopted our proposed UGST to obtain the low-frequency component $d(x,t,f_L)$ and high-frequency component $d(x,t,f_H)$. Finally, we utilized the difference between them to estimate the seismic attenuation result $\mathrm{SA}(x,t)$ qualitatively at the target layer $H_T(x)$, which is defined as **Equation (5)**:

$$\mathrm{SA}(x,t) = d(x,t,f_L) - \eta(x) \times d(x,t,f_H) \quad (5)$$

Where $\eta(x) = d(x,H_R(x),f_L)/d(x,H_R(x),f_H)$ is a scale-modified factor to remove the error behind the target layer. To enhance numerical stability when the high-frequency component amplitude is small, we applied a simple thresholding procedure. Before computing $\eta(x)$, the high-frequency amplitude was compared against a noise-level threshold T, which was derived from the average amplitude in non-reservoir intervals. If the amplitude fell below T, it

was replaced by T. This prevented division by near-zero values while maintaining the attenuation contrast essential for reservoir characterization. In this way, benefiting from the TF spectrum with high TF readability achieved by the proposed UGST, we effectively delineated seismic attenuation. In addition, the proposed UGST mitigates the frequency shift issue, which is beneficial to accurately characterize seismic attenuation.

3. Experimental setup

3.1. Field data and geological setting

The proposed UGST workflow was validated using 3D post-stacked seismic data from the Ordos Basin, Northwest China. This region represented a complex fault-block reservoir system developed in a fluvial-deltaic sedimentary environment. The target formation consisted of a series of thin interbedded sandstones and shales, with reservoir thickness typically below seismic tuning thickness, making it particularly challenging for conventional seismic interpretation methods. Understanding such complex reservoir systems benefited from insights gained in related geological studies, including investigations of pore-fracture connectivity in shale reservoirs[38] and fluid-rock interactions at the molecular scale.[39] These studies highlighted the importance of micro-scale features that influenced macro-scale seismic responses, providing context for interpreting the attenuation anomalies observed in our study. The structural framework was characterized by a series of northeast-southwest-trending normal faults that compartmentalize the reservoir into several isolated blocks.

The dataset covered an area of approximately 108 km^2 with a bin size of 20 m × 20 m, as indicated in Figure 2. The target interval spanned 2,000–3,022 ms, with a 2 ms sample interval providing sufficient temporal resolution for detailed spectral analysis. Figure 3 presents the normalized Fourier spectrum of the whole seismic data at the target layers. It is evident that the effective frequency bandwidth of the seismic data ranged from 5 Hz to 50 Hz, as determined from spectral analysis of multiple representative traces across the survey area. This comprehensive spectral analysis ensured that the selected frequency components for attenuation calculation fall within the reliable signal band, thereby enhancing the robustness of our attenuation estimation. Four key wells, spanning different structural positions, were selected for method validation (W1, W2, W3, and W4; Table 1). These wells provided comprehensive logging data, including gamma-ray, resistivity, and density logs, along with production test results that served as ground truth for validation of attenuation analysis.

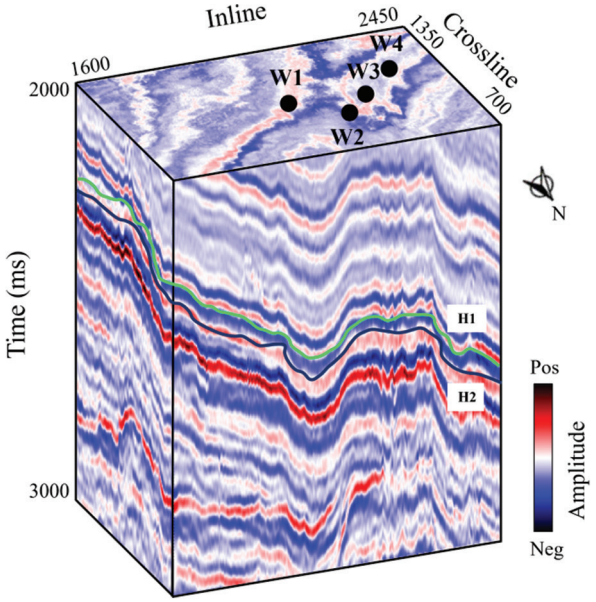

Figure 2. The three-dimensional post-stacked seismic data, located at the Ordos Basin, Northwest China, where W1, W2, W3, and W4 indicate four productive wells. The green and dark blue solid curves present two interpreted horizons: H1 and H2.

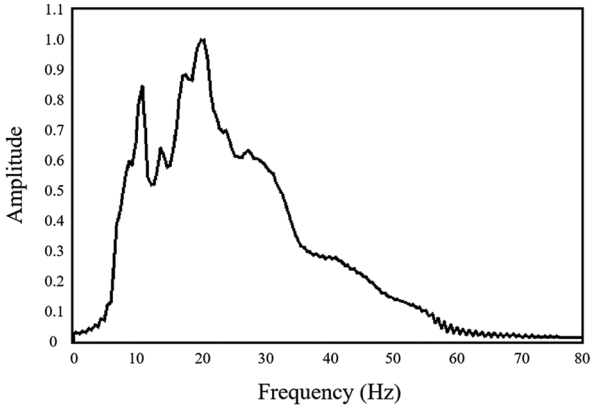

Figure 3. The normalized Fourier spectrum of the whole field data at the target layers

Table 1. Summary of well–borehole data used for validation

Well	Depth to reservoir (m)	Production rate (10^4 m^3/d)	Fluid type
W1	3,150–3,210	10.02	Gas
W2	3,190–3,220	6.45	Gas
W3	3,175–3,205	6.35	Gas
W4	3,200–3,220	1.73	Gas

3.2. Data preprocessing and parameter configuration

A comprehensive preprocessing sequence was applied to the seismic data before UGST analysis to ensure data quality

and interpretation reliability. Structural smoothing using dip-steered filtering was implemented to enhance lateral continuity while carefully preserving fault structures and stratigraphic terminations. This was particularly important given the complex fault network presented in the study area. Surface-consistent amplitude compensation was applied to normalize amplitude variations caused by near-surface effects and acquisition geometry, ensuring uniform seismic response across the entire survey area. Random noise suppression via FX-deconvolution improved the signal-to-noise ratio, a crucial for reliable TF analysis.

The design and parameterization of these preprocessing steps were carefully considered to balance noise suppression with the preservation of geological features. Specifically, dip-steered smoothing was applied with a conservative operator length (3 traces laterally, 5 ms vertically) to improve lateral continuity without blurring fault boundaries or stratigraphic terminations. This step was particularly critical in the fault-compartmentalized reservoirs of the Ordos Basin, where maintaining structural integrity was essential for reliable anomaly mapping. FX-deconvolution was employed to suppress random noise while preserving amplitude variations related to fluid content. Its parameters were calibrated to avoid over-smoothing, which could otherwise mask subtle attenuation anomalies associated with thin gas-bearing layers. The effectiveness of these preprocessing steps was validated by comparing raw and processed sections along key horizons, confirming that attenuation anomaly boundaries remained geologically consistent and aligned with well-based fluid indicators. Together, these preprocessing measures ensured that the input data to UGST were both interpretable and representative of true subsurface responses, thereby enhancing the reliability of the subsequent attenuation estimation without introducing artifacts or unrealistic smoothing.

The UGST parameters were optimized through an iterative testing process focused on achieving optimal TF resolution for the specific geological objectives. The window parameter k was set to 1.2 after testing values ranging from 0.5 to 2.0, with this value providing the best compromise between time and frequency resolution for the target thin-bed reservoirs. The scaling parameter p was established at 0.8, which was found to provide enhanced resolution in the low-frequency range while maintaining adequate time localization. Frequency selection was based on comprehensive spectral analysis of the entire seismic volume, as indicated in Figure 3, with the low frequency F_L set at 8 Hz and high frequency F_H at 34 Hz, both falling within the effective bandwidth of the data while providing sufficient separation for attenuation analysis. The careful selection of these frequencies, guided by the global spectrum, ensured that the attenuation calculation captured meaningful spectral variations related to reservoir properties. A continuous shale layer immediately above the target reservoir interval was selected as the reference horizon for amplitude normalization, ensuring that the resulting attenuation anomalies primarily reflected fluid-related effects rather than lithological variations.

The parameters k and p in the UGST formulation served distinct yet complementary roles in shaping the TF representation. k primarily controlled the width of the Gaussian window in the time domain, influencing the trade-off between temporal sharpness and frequency localization. k = 1.2 was selected after iterative testing across a range of 0.5–2.0. This choice was driven by the need to balance two competing demands in the Ordos Basin reservoirs: Sufficient temporal resolution to delineate thin interbedded layers (often below tuning thickness) and adequate frequency stability to reliably track attenuation trends. Lower k values (<1.0) improved temporal resolution but introduced undesirable spectral smearing in the low-frequency range, while higher k values (>1.5) enhanced frequency discrimination at the expense of blurring subtle temporal boundaries associated with fluid contacts. On the other hand, p modulated the window's shape in the frequency domain, effectively controlling how the window scaled with frequency. Setting p = 0.8 was found to optimize the representation of the seismic bandwidth relevant to attenuation analysis (approximately 5–50 Hz in this dataset). This value enhanced resolution in the lower frequency band (8–20 Hz), where gas-related attenuation anomalies were often most diagnostic, without over-compressing the window at higher frequencies where noise may dominate.

Together, these parameter choices reflected a tailored approach to the specific seismic response and geological complexity of the study area. The selection was further validated by comparing UGST outputs with well-log indicators across multiple representative traces, confirming that the chosen parameter set yielded TF spectra that were both interpretable and geologically consistent. While these values were optimized for the Ordos Basin dataset, the same methodological framework—iterative testing guided by local seismic character and geological objectives—could be applied to adapt UGST to other basin settings or data types.

3.3. Validation methodology

A multi-faceted validation approach was implemented to assess the reliability and geological consistency of the UGST-derived attenuation results. Well-based validation involved direct comparison of attenuation anomalies with known fluid contacts identified from well logs, with

particular focus on the gas–water contacts identified in W1 and W2. Production data correlation examined the relationship between attenuation strength and actual production performance, providing a practical measure of the method's predictive capability. Geological consistency assessment evaluated the spatial correlation between attenuation anomalies and structural features, ensuring that the observed patterns aligned with the understood petroleum system dynamics. Comparative analysis with conventional ST and UST implementations provided a baseline for evaluating the added value of the UGST approach, with particular attention to resolution improvement and frequency fidelity.

4. Results and discussions

4.1. TF analysis comparisons

To ensure a fair comparison among the TF methods, all transforms were implemented under consistent computational conditions. The standard ST and UST were implemented using their conventional formulations with Gaussian windows, matching the temporal sampling (2 ms) and frequency range (0–80 Hz) of UGST. No amplitude-preserving adjustments were applied to any method, ensuring that input data and processing conditions remained identical for all analyses. The TF characteristics of different transforms were examined using a representative seismic trace located near W1 (Figure 4A), which penetrated a known gas-bearing zone. The conventional ST result in Figure 4B displays a noticeable frequency shift phenomenon, with the dominant frequency appearing at approximately 45 Hz compared to the actual 35 Hz characteristic of the seismic wavelet. This systematic deviation introduced significant uncertainty in subsequent spectral decomposition and attenuation analysis. The UST result in Figure 4C successfully corrected this frequency shift but exhibited smeared TF representation, particularly in the critical 20–30 Hz range where important stratigraphic information was contained. The reduced concentration of spectral energy made it difficult to identify subtle features associated with thin bedding and fluid effects. In contrast, the UGST provided both accurate frequency localization and superior energy concentration (Figure 4D), clearly resolving the subtle spectral variations associated with thin layers and fluid contacts. The superior performance of UGST was particularly evident in the precise delineation of the frequency components around 30–40 Hz, which corresponded to the primary reservoir response, a feature that was blurred in both ST and UST results. The adjustable parameters enable optimal balancing of time and frequency resolution, revealing detailed features that are obscured in both ST and STFT representations.

4.2. Geological interpretation and discussions

Figure 5 displays the two-dimensional post-stacked seismic profile with four borehole locations (W1, W2, W3, and W4), where the yellow blocks clearly mark the reservoirs between two interpreted horizons: H1 and H2. All four wells penetrated gas-bearing reservoirs within

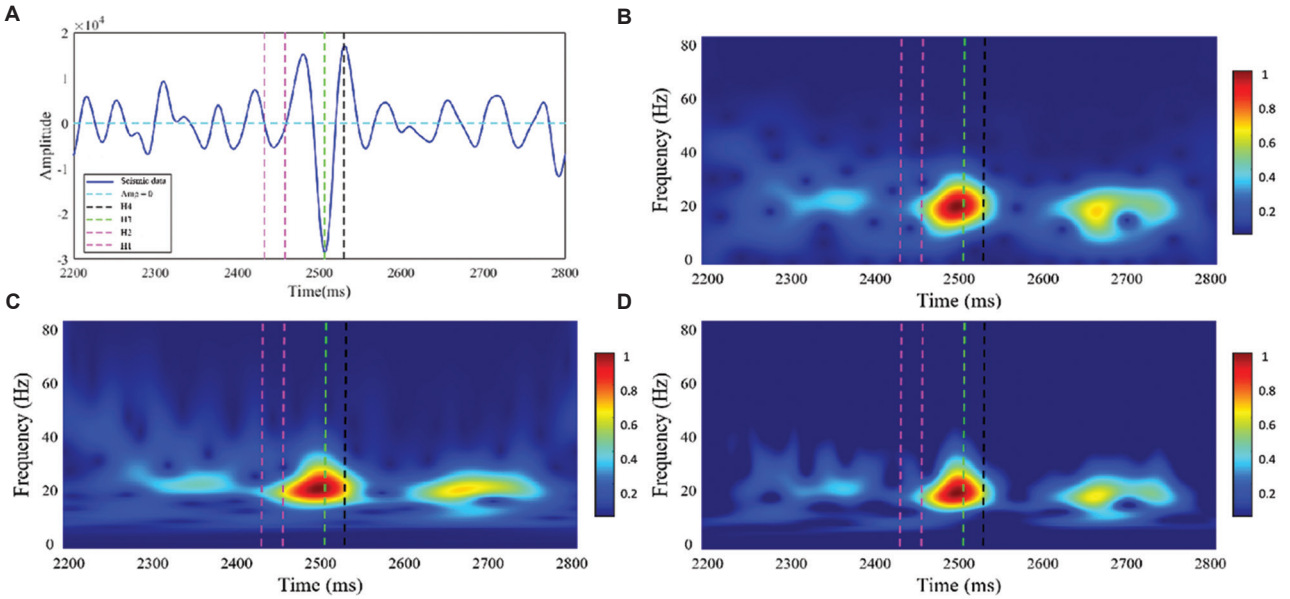

Figure 4. A representative seismic trace and its time-frequency spectra. (A) A representative seismic trace located near Well A and its time–frequency transform results calculated using (B) S-transform, (C) Unscaled S-transform, and (D) Unscaled generalized S-transform. The black, green, and two pink dashed lines indicate horizon H4, H3, H2, and H1, where the interpreted reservoir is located between H1 and H2.

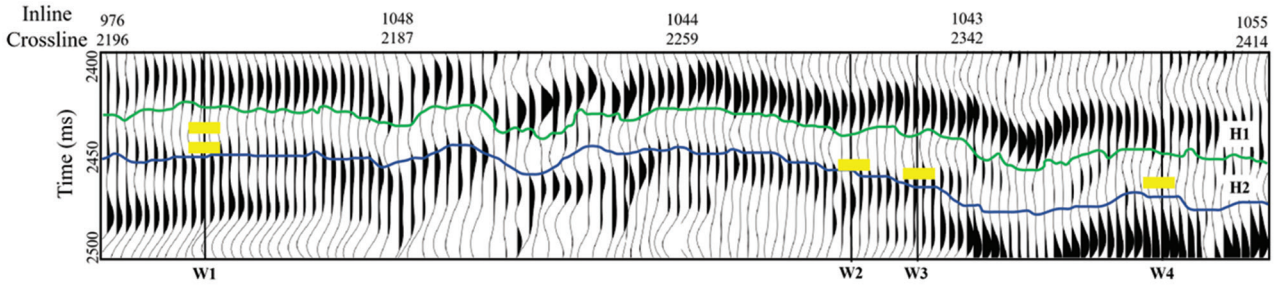

Figure 5. Two-dimensional post-stacked field data with four borehole locations. The green and dark blue solid curves present two interpreted horizons: H1 and H2. The yellow blocks indicate the location of the interested reservoirs.

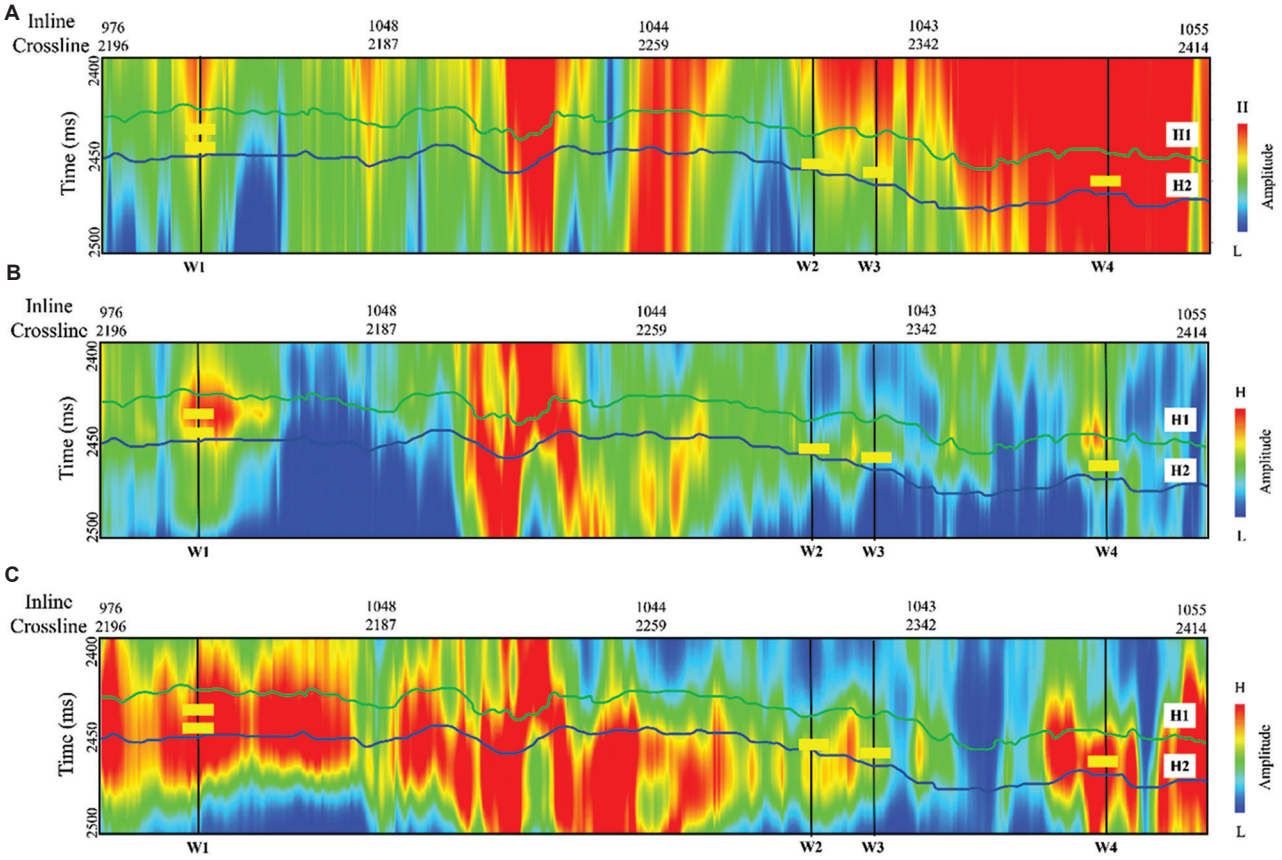

Figure 6. Seismic attenuation estimation for two-dimensional post-stacked field data in Figure 4, calculated by using (A) S-transform, (B) Unscaled S-transform, and (C) Unscaled generalized S-transform

these marked intervals, providing a robust dataset for method validation. The seismic profile shows characteristic reflection patterns typical of fluvial-deltaic depositional systems, with complex stratigraphic relationships and fault structures that pose challenges for conventional interpretation methods.

The qualitative attenuation profiles along target reservoirs demonstrated distinct characteristics among the three methods, as shown in Figure 6. The ST-based attenuation result in Figure 6A exhibits scattered anomalies with discontinuous spatial distribution, showing limited correlation with the known reservoir positions marked by yellow rectangles. The anomaly patterns appeared fragmented and lacked geological consistency, making it difficult to establish meaningful relationships with the reservoir distribution. The persistent frequency shift in ST likely contributed to this inconsistent performance, as the inaccurate spectral representation affected both the

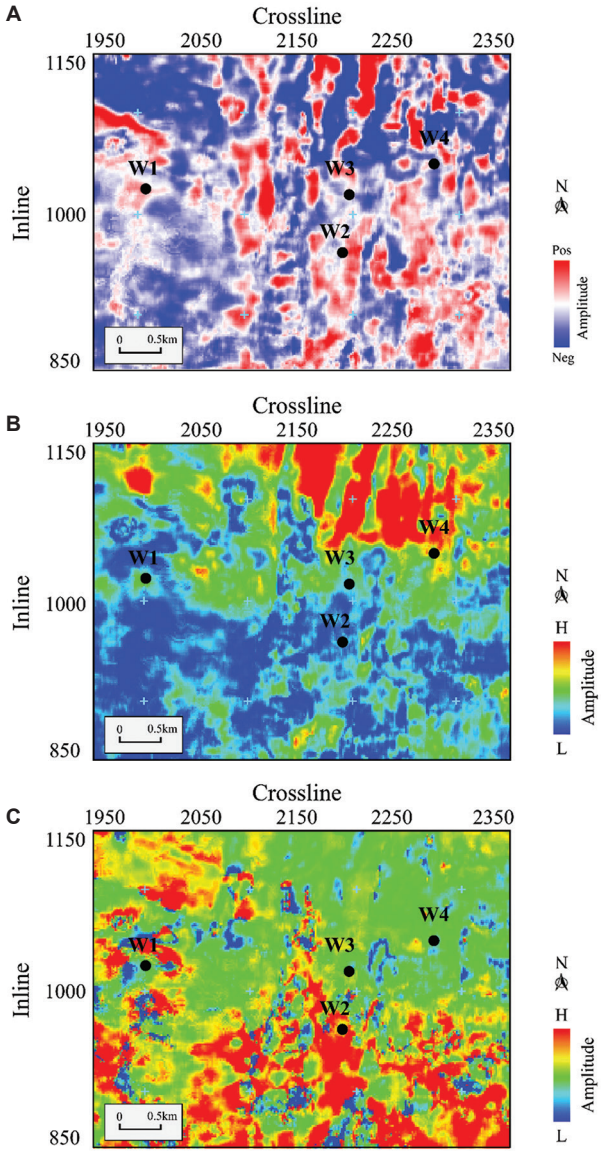

Figure 7. Seismic attribute slices extracted along H1 based on the post-stacked field data. (A) Seismic amplitude attribute. (B) Root mean square attribute. (C) Instantaneous frequency attribute.

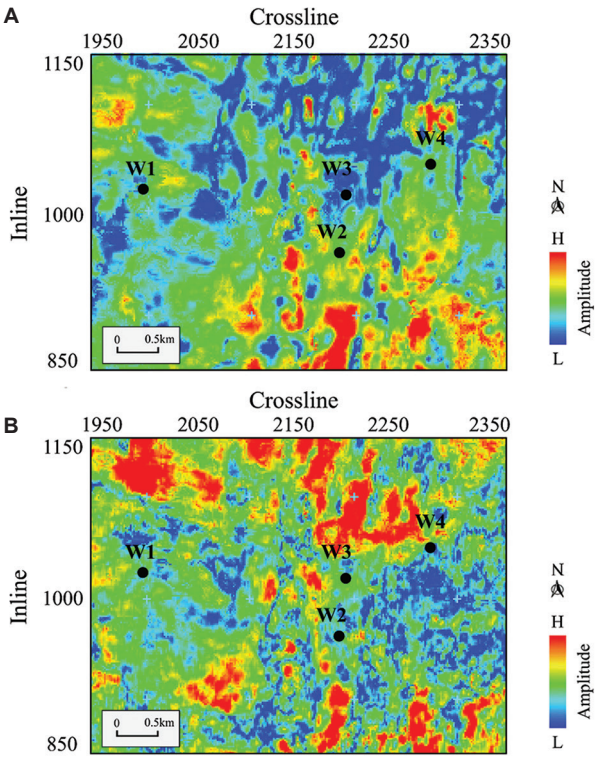

Figure 8. Constant frequency components extracted along H1 by using the S-transform; (A) low-frequency component and (B) high-frequency component.

low- and high-frequency components used in attenuation calculation. The UST-derived attenuation profile in Figure 6B shows improved spatial continuity compared to ST, with better-defined anomaly patterns that began to correlate with the reservoir positions. However, the resolution remained limited, particularly in delineating the detailed spatial variation of attenuation strength within the reservoir intervals. The anomalies appeared somewhat smoothed and lacked the sharp boundaries expected from geological considerations, suggesting that UST's fixed resolution limited its ability to capture fine-scale attenuation variations. The UGST-derived attenuation profile in Figure 6C reveals the most coherent and geologically consistent anomaly patterns among the three methods. The attenuation anomalies showed clear spatial correspondence with the reservoir positions marked by yellow rectangles, demonstrating strong correlation with all four gas-bearing wells (W1, W2, W3, and W4). The enhanced resolution of UGST effectively captured the attenuation variations within the reservoir units, showing well-defined anomaly boundaries that aligned with the structural and stratigraphic features observed in the seismic data. This improved performance was particularly evident in the areas between major faults, where UGST successfully identified continuous attenuation patterns that reflected the reservoir connectivity. Meanwhile, it is worth noting that the clear distinction between target and reference horizons in this study suggests a certain layer thickness, which typically improve detectability of gas-related attenuation contrasts. Nevertheless, the tunable resolution of UGST enabled it to capture subtle attenuation anomalies even in thinner reservoirs near or below seismic tuning thickness. This adaptability makes the method applicable not only to thick gas-bearing intervals but also to challenging thin-bed environments where conventional methods often struggle.

A comparative summary of the three methods highlights the quantitative improvements UGST offered. In terms of frequency fidelity, both UST and UGST fully corrected the approximately 10 Hz systematic shift observed in ST (Figure 4). Regarding the spatial consistency of anomalies, visual analysis of the attenuation profiles (Figure 6) indicated that UGST produced continuous anomalies that corresponded to all four validation wells, a level of alignment not achieved by the fragmented ST result. Furthermore, UGST demonstrated superior resolution in delineating reservoir boundaries within the target interval, as evidenced by sharper attenuation anomaly definition compared to the smeared responses of ST and UST. While formal cross-well correlation coefficients are beyond the scope of this qualitative case study, the consistent and enhanced performance of UGST across these multiple, observable criteria strongly supports its practical utility for attenuation-based reservoir characterization.

For the 3D seismic analysis, all attribute extractions were performed along the H1 horizon. H1 was selected for 3D attribute extraction because it corresponded to the top of the main reservoir unit within the 2,000–3,022 ms target interval. Seismic interpretation confirmed that the primary gas-bearing reservoirs are predominantly developed immediately beneath this surface, making H1 the most suitable reference for mapping reservoir–related attenuation anomalies throughout the 3D volume. This alignment ensured that the observed attenuation patterns were directly linked to the primary reservoir development zone, enhancing the geological relevance of our interpretations. This approach was adopted because seismic interpretation confirmed that the main reservoir units were predominantly developed adjacent to the H1 surface, making it the most suitable reference for mapping reservoir-related attenuation anomalies throughout the 3D volume. The choice of H1 for 3D attribute extraction thus directly linked the observed attenuation anomalies to the primary reservoir development zone, improving the geological relevance of our interpretations. Further analysis of seismic attribute slices along horizon H1 provided additional geological context for interpreting the attenuation results, as shown in Figure 7. The seismic amplitude attribute in Figure 7A reveals the basic structural framework, showing fault patterns and stratigraphic features that control the reservoir distribution. The root-mean-square amplitude attribute in Figure 7B enhances

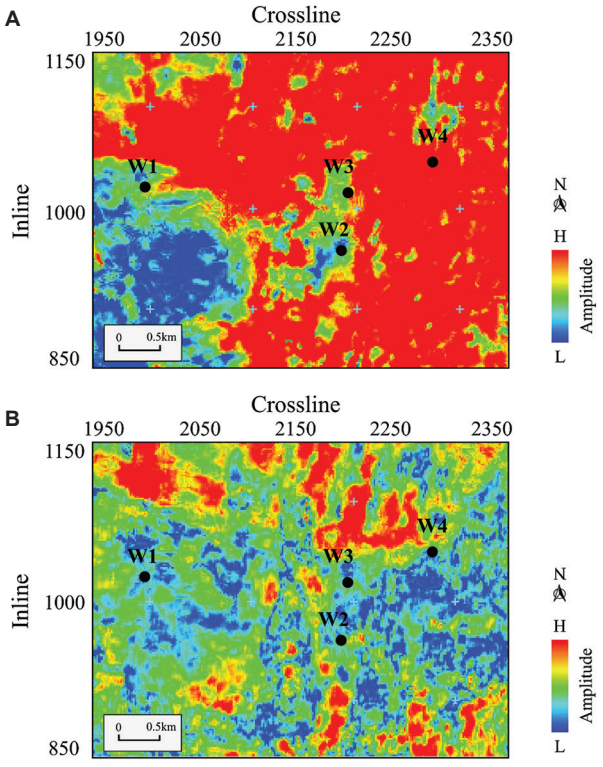

Figure 9. Constant frequency components extracted along H1 by using the unscaled S-transform; (A) low-frequency component and (B) high-frequency component

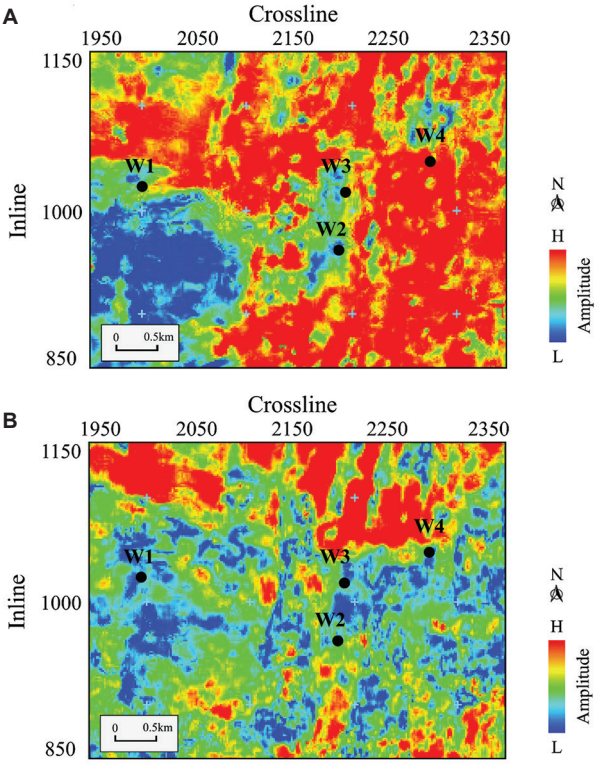

Figure 10. Constant frequency components extracted along H1 by using the unscaled generalized S-transform; (A) low-frequency component and (B) high-frequency component

the identification of amplitude anomalies associated with reservoir properties, showing good correlation with the known gas-bearing zones. The instantaneous frequency attribute in Figure 7C shows complementary spectral characteristics that supported the attenuation analysis, with frequency anomalies that corresponded well to the attenuation patterns identified by UGST.

We extracted and compared the constant-frequency components calculated using ST, UST, and UGST, as indicated in Figures 8-10, respectively. The subplots (A) and (B) denote the low- and high-frequency components extracted along the interpreted horizon H1.

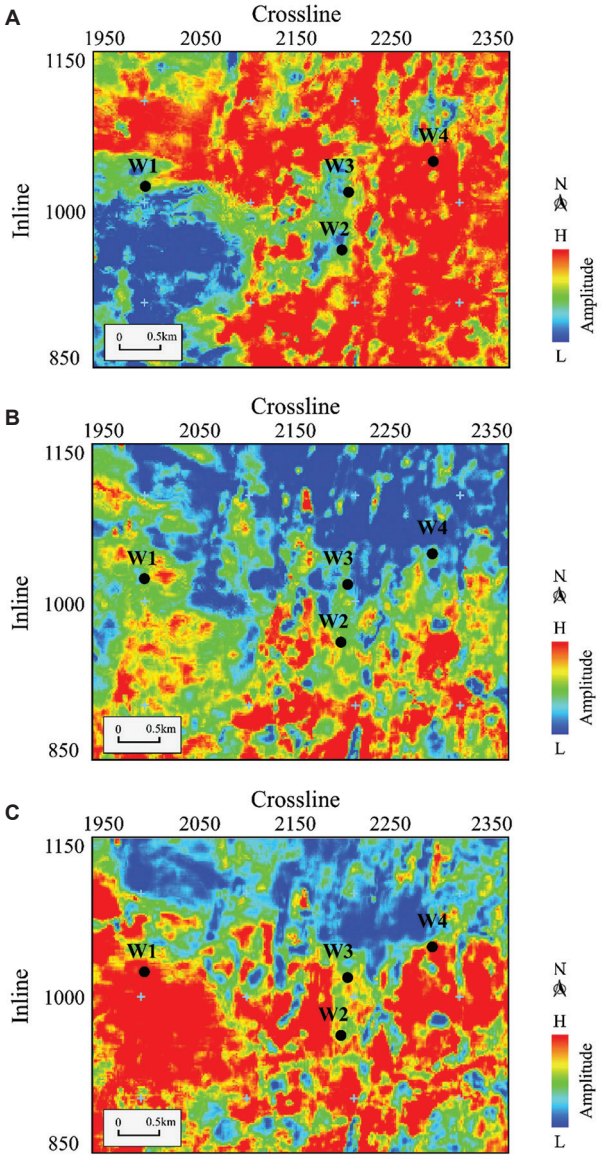

Figure 11. Seismic attenuation slices of H1 in 3D field data calculated by using (A) S-transform, (B) unscaled S-transform, and (C) unscaled generalized S-transform, respectively

We selected 8 Hz and 34 Hz as the low- and high-frequency bands in this study based on the Fourier spectrum of the whole field data. By comparing these images, we found that the components extracted using ST in Figure 8 showed significant spectral smearing and resolution limitations, particularly in the high-frequency component, where geological details were obscured by the method's inherent limitations. The UST-derived components in Figure 9 provided improved frequency fidelity, but resolution was limited in complex areas, limiting the ability to separate thin layers and subtle features. In contrast, our UGST method Figure 10 delivered superior component separation with enhanced resolution, clearly delineating the reservoir boundaries and internal heterogeneities that are critical for accurate reservoir characterization. It can be concluded that the constant-frequency component analysis demonstrated UGST's advantage in reservoir characterization through detailed comparisons of the extracted low- and high-frequency components.

Finally, we calculated and extracted the comprehensive 3D attenuation results as shown in Figure 11. Figure 11A-C correspond to the results calculated using ST, UST, and UGST, respectively. The UGST-derived attenuation slice showed well-defined anomaly patterns that correlated strongly with the reservoir distribution, whereas the results from ST and UST exhibited progressively poorer resolution and anomaly definition. The spatial continuity of UGST anomalies provided valuable insights into reservoir connectivity and compartmentalization, with attenuation patterns that reflected the complex interplay between structural elements and fluid distribution. The application of UGST for qualitative attenuation estimation in this complex reservoir confirmed its value for characterizing reservoirs under challenging geological conditions. The method's ability to accurately localize frequency while maintaining flexible resolution control addresses the fundamental limitations of conventional TF approaches. The strong correlation between UGST-derived attenuation anomalies and known reservoir positions, combined with the method's enhanced resolution, highlighted its potential to reduce exploration risk and improve reservoir characterization accuracy in similar complex reservoir settings. The consistent performance across different geological scenarios and the ability to reveal meaningful attenuation patterns that align with known geological features made UGST a valuable tool for integrated seismic interpretation and reservoir characterization workflows.

The UGST-derived attenuation maps provided high-resolution delineation of fluid-bearing zones, which can directly guide future well placement. For instance, areas with strong and continuous attenuation anomalies

along H1 (e.g., between W1 and W2) represent promising targets for infill drilling. In addition, the method's ability to resolve compartmentalization enabled optimization of injection strategies for enhanced oil recovery by identifying barriers and conduits within the reservoir. These insights reduced drilling uncertainty and support data-driven field development planning.

5. Conclusion

Our study presents the application of the UGST for qualitative estimation of seismic attenuation in a complex fault-block reservoir in the Ordos Basin, China. The proposed method effectively addressed two fundamental limitations of conventional TF analysis techniques: The systematic dominant-frequency shift inherent in the standard ST and the fixed resolution characteristics of the UST. By introducing tunable parameters into the Gaussian window function, UGST provides flexible control over TF resolution while maintaining accurate frequency representation, enabling enhanced analysis of non-stationary seismic signals.

The field application demonstrated that UGST generated TF spectra with superior readability and resolution compared to both conventional ST and UST methods. More importantly, the qualitative attenuation profiles derived from UGST showed strong correlation with known gas-bearing zones confirmed by well logs and production data. The method successfully identified attenuation anomalies associated with hydrocarbon presence while providing improved resolution of thin reservoir units and complex fault compartments. The geological consistency of the results, particularly the spatial alignment between attenuation anomalies and structural features, confirms the method's reliability for reservoir characterization in geologically complex settings.

The workflow developed in this study offers a robust approach for identifying fluid-related attenuation effects while minimizing interference from lithological variations. The identification of previously unrecognized prospective areas highlights UGST's potential to reduce exploration risk and optimize development strategies in similar complex reservoir environments. The principles underlying UGST-based attenuation analysis extend beyond hydrocarbon exploration to various geotechnical and engineering applications. In near-surface and engineering geophysics, similar TF approaches have been employed for tunnel seismic prospecting[40] and ground deformation monitoring using InSAR data.[41] Furthermore, in seismic hazard assessment, the accurate characterization of seismic signals is crucial for selecting appropriate ground motion models.[42] These diverse applications demonstrate the broad relevance of high-resolution signal analysis techniques across different scales and problem domains. The suggested UGST can be easily converted to a sparse version,[33] sacrificing computational efficiency for TF resolution. Due to our limited knowledge and the requirements of this research for efficient computation, we do not extend our suggested transform to the sparse version. Future work should focus on extending the method to the sparse version and on its application to quantitative attenuation estimation. We can also integrate it with other seismic attributes for comprehensive reservoir characterization. Moreover, the UGST method is not limited to the Ordos Basin and can be adapted to other sedimentary basins with complex reservoir architectures, such as fluvial-deltaic, turbidite, or carbonate systems. Its flexible parameterization allows customization for varying seismic data characteristics, including different frequency bandwidths, signal-to-noise ratios, and wavelet properties.

Acknowledgments

None.

Funding

This research was supported by the Science and Technology Projects of Yumen Oilfield Company for 2024–2025 (Grant No. YM2024-001).

Conflict of interest

The authors declare that they have no competing interests.

Author contributions

Conceptualization: Wenlong Jiao, Yongxiang Jiang
Formal analysis: Yongxiang Jiang
Investigation: Jun Yang, Wei Zhao
Methodology: Wenlong Jiao, Naihao Liu
Validation: Jun Yang, Wei Zhao
Writing–original draft: Wenlong Jiao, Wei Zhao
Writing–review & editing: Naihao Liu

Availability of data

Data are available on request through naihao_liu@mail.xjtu.edu.cn.

References

1. Li F, Verma S, Zhou H, Zhao T, Marfurt KJ. Seismic attenuation attributes with applications on conventional and unconventional reservoirs. *Interpretation*. 2016;4(1):SB63-SB77.

   doi: 10.1190/INT-2015-0105.1

2. Wang Z, Gao J, Wang D, Wei Q. 3D seismic attributes for a tight gas sand reservoir characterization of the eastern Sulige gas field, Ordos Basin, China. *Geophysics*. 2015;80(2):B35-B43.

doi: 10.1190/geo2014-0362.1

3. Ba J, Ba XY, Dong HJ, *et al*. Reservoir property estimation of interbedded sandstone and shale layers using segmented 3D rock-physics templates. *Appl Geophys*. 2025;22(3):1-17.

   doi: 10.1007/s11770-025-1263-3

4. Ashcroft W. Seismic input to mapping reservoir properties. In: *A Petroleum Geologist's Guide to Seismic Reflection*. United States: John Wiley and Sons; 2011. p. 127-145.

5. Liu S, Gu H, Yan Z, Li H, Wang H. Q-compensated beam migration with multiscale Gabor transform. *J Appl Geophys*. 2017;143:195-202.

   doi: 10.1016/j.jappgeo.2017.06.006

6. Ao Y, Li H, Zhu L, Ali S, Yang Z. Identifying channel sand-body from multiple seismic attributes with an improved random forest algorithm. *J Pet Sci Eng*. 2019;173:781-792.

   doi: 10.1016/j.petrol.2018.10.048

7. Ao Y, Li H, Zhu L, Yang Z. A SCiForest based semi-supervised learning method for the seismic interpretation of channel sand-body. *J Appl Geophys*. 2019;167:51-62.

   doi: 10.1016/j.jappgeo.2019.04.019

8. Wang Z, Gao J, Lei X, Cui X, Wang D. Application of 3D seismic attributes to optimize the placement of horizontal wells within a tight gas sand reservoir, Ordos Basin, China. *Geophysics*. 2016;81(3):B77-B86.

   doi: 10.1190/geo2015-0244.1

9. Chen Y, Liu T, Chen X, Li J, Wang E. Time-frequency analysis of seismic data using synchrosqueezing wavelet transform. In: *SEG Technical Program Expanded Abstracts 2014*. United States: Society of Exploration Geophysicists; 2014. p. 1589-1593.

   doi: 10.1190/segam2014-0034.1

10. Wang Y. The W transform. *Geophysics*. 2021;86(1):V31-V39.

    doi: 10.1190/geo2020-0316.1

11. Reine C, Van Der Baan M, Clark R. The robustness of seismic attenuation measurements using fixed-and variable-window time-frequency transforms. *Geophysics*. 2009;74(2):WA123-WA135.

    doi: 10.1190/1.3043726

12. Wang X, Gao J, Chen W, Zhao W, Jiang X, Zhu Z. Seismic attenuation qualitative characterizing method based on adaptive optimal-kernel time-frequency representation. *J Appl Geophys*. 2013;89:125-133.

    doi: 10.1016/j.jappgeo.2012.12.006

13. Wang B, Lu W. An efficient amplitude-preserving generalized S transform and its application in seismic data attenuation compensation. *IEEE Trans Geosci Remote Sens*. 2017;56(2):859-866.

    doi: 10.1109/TGRS.2017.2755666

14. Sinha S, Routh PS, Anno PD, Castagna JP. Spectral decomposition of seismic data with continuous wavelet transform. *Geophysics*. 2005;70(6):P19-P25.

    doi: 10.1190/1.2127113

15. Huang NE, Shen Z, Long SR, *et al*. The empirical mode decomposition and the Hilbert spectrum for nonlinear and non-stationary time series analysis. *Proc R Soc A*. 1998;454(1971):903-995.

    doi: 10.1098/rspa.1998.0193

16. Wang P, Gao J, Wang Z. Time-frequency analysis of seismic data using synchrosqueezing transform. *IEEE Geosci Remote Sens Lett*. 2014;11(12):2042-2044.

    doi: 10.1109/LGRS.2014.2317578

17. Liu N, Wei S, Li S, Yang Y, Zhang Y, Gao J. Sparse unscaled time-frequency transform and its application on seismic attenuation delineation. *Geophysics*. 2023;88(6):B355-B368.

    doi: 10.1190/geo2022-0522.1

18. Gholami A. Sparse time-frequency decomposition and some applications. *IEEE Trans Geosci Remote Sens*. 2012;51(6):3598-3604.

    doi: 10.1109/TGRS.2012.2220144

19. Liu N, Wei S, Liu R, Yang Y, Zhang N, Gao J. Seismic attenuation estimation via unscaled time-frequency representation and divergence. *IEEE Trans Geosci Remote Sens*. 2022;60:1-10.

    doi: 10.1109/TGRS.2022.3223721

20. Fu J, He T, Guo C, Bao Y, Li X, Liu X. An additional structure with power-law thickness for weak acoustic emission signal enhancement. *Thin Walled Struct*. 2025;211:113071.

    doi: 10.1016/j.tws.2025.113071

21. Li Z, Xie F, Ma J, Qi Z, Wang Y. CNN-based adaptive subtraction for the removal of seismic multiples. *J Seismic Explor*. 2023;32(2):169-184.

22. Liu N, Gao J, Zhang B, Wang Q, Jiang X. Self-adaptive generalized S-transform and its application in seismic time-frequency analysis. *IEEE Trans Geosci Remote Sens*. 2019;57(10):7849-7859.

    doi: 10.1109/TGRS.2019.2916792

23. Wang B. An amplitude preserving S-transform for seismic data attenuation compensation. *IEEE Signal Process Lett*. 2016;23(9):1155-1159.

    doi: 10.1109/LSP.2016.2586445

24. Verma AK, Cheadle BA, Mohanty WK, Routray A, Mansinha L. *Detecting Stratigraphic Discontinuities using Wavelet and S-Transform Analysis of Well Log Data*. In: *Proceedings of the GeoConvention 2012: Vision*; 2012. Calgary, Canada. Available from: https://geoconvention.

com/wp/content/uploads/abstracts/2012/163_gc2012_detecting_stratigraphic_discontinuities.pdf [Last accessed on 2026 Jan 16].

25. Shi Y, Zhou H, Niu C, Liu CC, Meng LJ. A variable gain-limited inverse Q filtering method to enhance the resolution of seismic data. *J Seismic Explor*. 2019;28:257-276.

26. Stockwell RG, Mansinha L, Lowe RP. Localization of the complex spectrum: The S transform. *IEEE Trans Signal Process*. 1996;44(4):998-1001.

doi: 10.1109/78.492555

27. Pinnegar CR, Eaton DW. Application of the S transform to prestack noise attenuation filtering. *J Geophys Res Solid Earth*. 2003;108(B9):2422.

doi: 10.1029/2002JB002258

28. Li D, Castagna J, Goloshubin G. Investigation of generalized S-transform analysis windows for time-frequency analysis of seismic reflection data. *Geophysics*. 2016;81(3):V235-V247.

doi: 10.1190/geo2015-0551.1

29. Beuter C, Oleskovicz M. S-transform: From main concepts to some power quality applications. *IET Signal Process*. 2020;14(3):115-123.

doi: 10.1049/iet-spr.2019.0042

30. Wu L, Castagna J. S-transform and Fourier transform frequency spectra of broadband seismic signals. *Geophysics*. 2017;82(5):O71-O81.

doi: 10.1190/geo2016-0679.1

31. Han C. Spectral decomposition AVO attributes for identifying potential hydrocarbon-related frequency anomalies. *First Break*. 2019;37(5):89-97.

doi: 10.3997/1365-2397.n0027

32. Li F, Zhou H, Zhao T, Marfurt KJ. Unconventional reservoir characterization based on spectrally corrected seismic attenuation estimation. *J Seismic Explor*. 2016;25(5):447-461.

33. Sattari H. High-resolution seismic complex trace analysis by adaptive fast sparse S-transform. *Geophysics*. 2017;82(1):V51-V67.

doi: 10.1190/geo2015-0425.1

34. Fomel S. Local seismic attributes. *Geophysics*. 2007;72(3):A29-A33.

doi: 10.1190/1.2437573

35. Liu J, Marfurt KJ. Instantaneous spectral attributes to detect channels. *Geophysics*. 2007;72(2):P23-P31.

doi: 10.1190/1.2428268

36. Yang Y, Gao J, Wang Z, Li Z. Seismic absorption qualitative indicator via sparse group-lasso-based time-frequency representation. *IEEE Geosci Remote Sens Lett*. 2021;18(9):1680-1684.

doi: 10.1109/LGRS.2020.3006340

37. Tary JB, Van Der Baan M, Herrera RH. Applications of high-resolution time-frequency transforms to attenuation estimation. *Geophysics*. 2017;82(1):V7-V20.

doi: 10.1190/geo2016-0022.1

38. Sun M, Duan X, Liu Q, *et al*. The importance of pore-fracture connectivity in overmature marine shale for methane occurrence and transportation. *Mar Pet Geol*. 2023;157:106495.

doi: 10.1016/j.marpetgeo.2023.106495

39. Yan Z, Wang F, Liu Y, Zhang J, Liu L, Gao M. Effects of CO_2 pressure on the dynamic wettability of the kerogen surface: Insights from a molecular perspective. *Appl Surf Sci*. 2025;694:162822.

doi: 10.1016/j.apsusc.2025.162822

40. Jia C, Cheng S, Li L, Chen Y. Seismic ahead-prospecting method based on delayed blasting excitation in the tunnel face: A case study. *Tunnell Undergr Space Technol*. 2025;161:106577.

doi: 10.1016/j.tust.2025.106577

41. Liang Y, Qiu H, Wang J, *et al*. Automated identification of ground kinematic patterns based on InSAR time series displacement and K-SC clustering. *Eng Geol*. 2025;357:108367.

doi: 10.1016/j.enggeo.2025.108367

42. Li B. Selecting hazard-consistent ground motions for seismic risk analysis: An equivalent earthquake-based methodology. *Bull Earthq Eng*. 2025;23:5275-5299.

doi: 10.1007/s10518-025-02228-4